Remote Sens. **2013**, *5*, 3872-3895; doi:10.3390/rs5083872

OPEN ACCESS

Remote Sensing

ISSN 2072-4292

www.mdpi.com/journal/remotesensing

Article

Spectrometer for Sky-Scanning Sun-Tracking Atmospheric Research (4STAR): Instrument Technology

Stephen E. Dunagan [1,*], Roy Johnson [1], Jhony Zavaleta [1], Philip B. Russell [1], Beat Schmid [2], Connor Flynn [2], Jens Redemann [1], Yohei Shinozuka [3,4], John Livingston [5] and Michal Segal-Rosenhaimer [1]

[1] Ames Research Center, NASA, MS 245-4, Moffett Field, CA 94035, USA; E-Mails: Roy.R.Johnson@nasa.gov (R.J.); Jhony.R.Zavaleta@nasa.gov (J.Z.); Philip.B.Russell@nasa.gov (P.B.R.); Jens.Redemann-1@nasa.gov (J.R.); Michal.Segalrozenhaimer@nasa.gov (M.S.-R.)

[2] Pacific Northwest National Laboratory, Richland, WA 99325, USA; E-Mails: beat.schmid@pnnl.gov (B.S.); connor.flynn@pnnl.gov (C.F.)

[3] The Ames Cooperative for Research in Earth Science and Technology (ARC-CREST), NASA, Moffett Field, CA 94035, USA; E-Mail: Yohei.Shinozuka@nasa.gov

[4] Bay Area Environmental Research Institute, Sonoma, CA 95476, USA

[5] SRI International, 333 Ravenswood Avenue, Menlo Park, CA 94025, USA; E-Mail: John.M.Livingston@nasa.gov

* Author to whom correspondence should be addressed; E-Mail: Stephen.E.Dunagan@nasa.gov; Tel.: +1-650-604-4560; Fax: +1-650-604-4680.

Received: 14 June 2013; in revised form: 22 July 2013 / Accepted: 23 July 2013 / Published: 6 August 2013

Abstract: The Spectrometer for Sky-Scanning, Sun-Tracking Atmospheric Research (4STAR) combines airborne sun tracking and sky scanning with diffraction spectroscopy to improve knowledge of atmospheric constituents and their links to air-pollution/climate. Direct beam hyper-spectral measurement of optical depth improves retrievals of gas constituents and determination of aerosol properties. Sky scanning enhances retrievals of aerosol type and size distribution. 4STAR measurements will tighten the closure between satellite and ground-based measurements. 4STAR incorporates a modular sun-tracking/ sky-scanning optical head with fiber optic signal transmission to rack mounted spectrometers, permitting miniaturization of the external optical head, and future detector evolution. Technical challenges include compact optical collector design, radiometric dynamic range and stability, and broad spectral coverage. Test results establishing the performance of the instrument against

the full range of operational requirements are presented, along with calibration, engineering flight test, and scientific field campaign data and results.

Keywords: atmosphere; climate; pollution; radiometry; technology; hyperspectral; fiber optic

1. Introduction

Since 1985, National Aeronautics and Space Administration (NASA) Ames Airborne Tracking Sunphotometers (AATS-6 and -14) have made extensive measurements of atmospheric constituents via their effect on the Sun's direct-beam transmission through the atmosphere. Constituents measured to date include aerosols (e.g., [1]), H_2O [2], and O_3 [3]. AATS measurements are used extensively to validate and supplement satellite retrievals of stratospheric and tropospheric constituents [4], validate airborne and ground-based lidar data products [5], characterize horizontal and vertical distributions of gas and aerosol properties [6], study closure (consistency) with *in situ* samplers aboard many aircraft (e.g., [7]), test chemical-transport models [8], and study the radiative effects of atmospheric constituents and Earth surfaces that are important to both climate and remote measurements [9]. AATS measurements and analyses are described in more than 100 publications since 1987 [10].

Figure 1. Features of Spectrometer for Sky Scanning Sun-Tracking Atmospheric Research (4STAR) as related to Ames Airborne Tracking Sunphotometer (AATS)-14 and AErosol RObotic NETwork (AERONET).

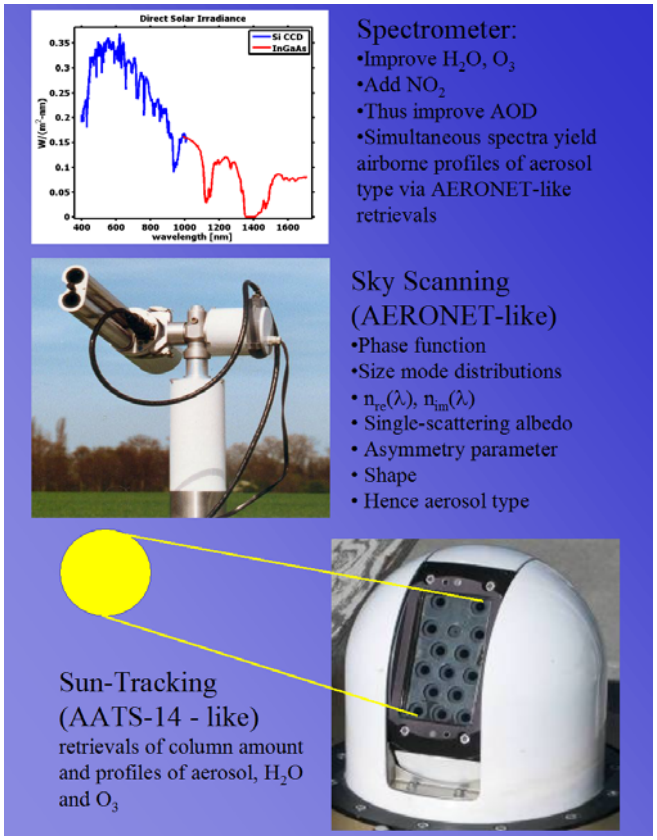

The NASA Ames Sun-photometer-Satellite Group, the Department of Energy (DOE) Pacific Northwest National Laboratory's (PNNL) Atmospheric Sciences and Global Change Division, and NASA Goddard's AERONET (AErosol RObotic NETwork) team have collaborated on the development of a new airborne sunphotometry instrument that will provide information on gases and aerosols extending far beyond what can be derived from discrete-channel direct-beam measurements, while preserving or enhancing many of the desirable AATS features (e.g., compactness, versatility, automation, reliability). The enhanced instrument combines the sun-tracking ability of the current 14-Channel NASA Ames AATS-14 with the sky-scanning ability of the ground-based AERONET Sun/sky photometers, while extending both AATS-14 and AERONET capabilities by providing full spectral information from the UV (350 nm) to the SWIR (1,700 nm) as represented in Figure 1. A more detailed view of spectral measurement capability with respect to AATS as well as aerosol extinction and gas constituent absorption features is presented in Figure 2. Strengths of this measurement approach include many more wavelengths (isolated from gas absorption features) that may be used to characterize aerosols and detailed (oversampled) measurements of the absorption features of specific gas constituents.

Figure 2. Wavelength ranges and resolutions of the two Spectrometer for Sky Scanning Sun-Tracking Atmospheric Research (4STAR) spectrometers in relation to Ames Airborne Tracking Sunphotometer (AATS)-14 channel wavelengths (vertical lines with arrows) and atmospheric spectra. δλ = spacing of pixel centers; Δλ = slit/diffraction limited full width at half maximum (FWHM). The spectra of transmittance T of the direct solar beam at sea level were calculated using MODTRAN-4.3 with a Midlatitude Summer atmosphere, a rural spring-summer tropospheric aerosol model (Vis = 23 km), and the sun at the zenith. Assumed O_3 = 332 DU, NO_2 = 0.22 DU.

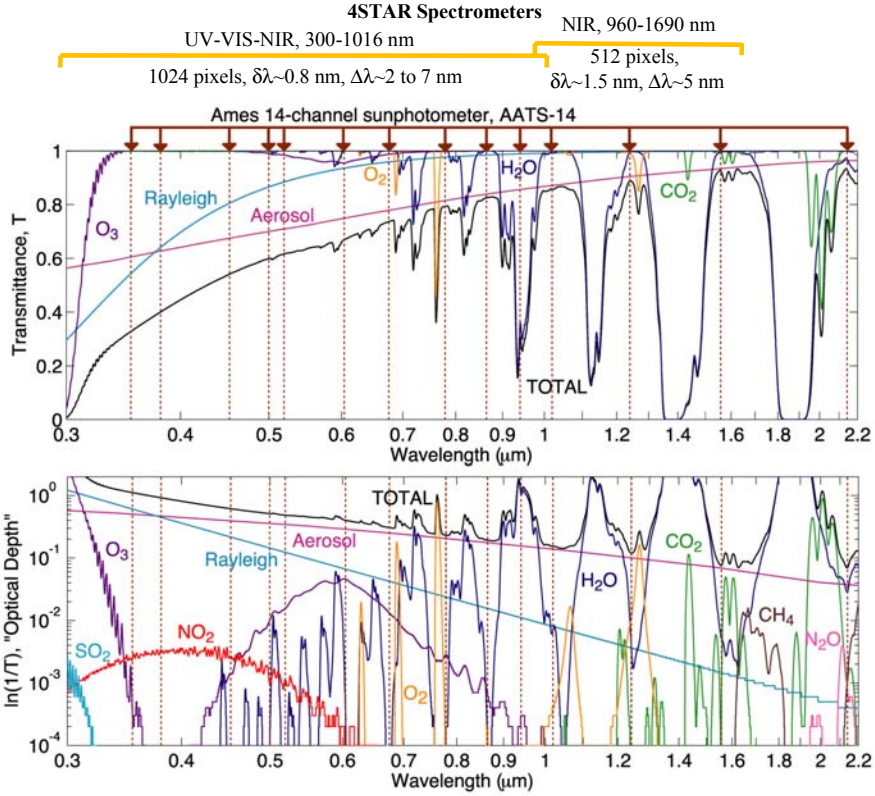

2. Instrument Description

Previous AATS designs were based on a number of optoelectronic modules, each comprising a spectral-band interference filter covering a photodiode detector, with amplifier and digitizer circuitry interfaced to a data acquisition system, all built into the instrument body. A 2-axis motion control system with analog feedback control and DC servomotor actuators provided tracking of the solar disk to permit very stable radiometric measurements with negligible variability from tracking errors. 4STAR retains similar sun tracking requirements but represents a major departure from this design for nearly all other instrument subsystems.

The most fundamental improvement derives from the science requirement for higher spectral resolution to resolve gas absorption features, and provide continuous, high-resolution measurements across the spectrum. Advances in diffraction spectrometer designs have made it possible to specify commercial spectrograph and detector combinations that will meet 4STAR requirements for resolution and dynamic range. Two spectrometers are required to cover the full 350 to 1,700 nm spectral range.

Fiber optic bundle fore-optics are commonly implemented with field spectrometers, and represent a straightforward choice for the 4STAR light collection system. A flexible bundle can be easily manipulated to track the sun or scan the sky, and the small input aperture is readily adapted to miniaturized baffled Gershun tubes [11] that properly limit the instrument field of view.

Recent improvements in industrial-grade motion control equipment permit the specification of packaged stepping-motor/driver and feedback sensors that can meet the high pointing accuracy and modest dynamic response requirements for the instrument. Finally, digital controller and data acquisition elements permit replacement of virtually all analog circuitry in the system with PC-based hardware that is readily programmed from a graphical user interface. The single element in the 4STAR that persists from earlier AATS designs is the quadrant photodiode detector that provides the differential analog signal to track the sun.

4STAR functional requirements to meet the scientific goals for the instrument are summarized in Table 1.

Several key questions arise in considering the transition to the new technology solutions outlined above:

1. Are the charge-coupled device (CCD) (quantum) detector elements capable of meeting the radiometric accuracy and stability required?
2. Does the combination of small aperture fiber optics and aggressive spectral dispersion within the spectrograph permit adequate light collection to meet the signal-to-noise ratio (SNR) requirement, *i.e.*, can photo-electrons be collected fast enough to get useful sky scan measurements within an acceptably small spatial domain?
3. Are stray light artifacts internal to the spectrometers adequately controlled (or deterministically correctable)?
4. Will a flexible fiber optic bundle and fiber optic rotary joint (FORJ) provide consistent radiometric transmission through the full range of motion?
5. Will the optical collectors' windows remain clean enough during flight experiments that data will not be unacceptably contaminated?

6. Can the mechanical motion axes be properly sealed across the aircraft pressure barrier without limiting tracking response?

Table 1. Summary of requirements.

Spectral	**Range**	**Resolution**
visible/near infrared (VNIR)	350 to 1,015 nm	2–3 nm
short wave infrared (SWIR)	900 to 1,700 nm	5–10 nm
Angular Sampling	**Range**	**FOV**
Direct solar beam	full hemisphere	1.25 deg
sky light	full hemisphere	2 deg
Pointing Control	**Range**	**Accuracy**
elevation	0 to 180 degrees	0.2 deg
azimuth	many revolutions	0.2 deg
Signal Amplitude		
Dynamic range	10^4	
Repeatability	<1.0% over 6 months	
Operational		
space (time)* to acquire direct beam data	100 m	
space (time)* to acquire sky scan data	10,000 m	
aircraft pitch, roll, and yaw rate tracking limits	6 deg/s	
aircraft climb and bank angle limits	25 deg	
altitude ceiling	12,500 m	

*space divided by airspeed provides time requirement

These technical challenges have been addressed through the development and testing of several prototype instruments. An initial ground-based proof-of-concept design was developed to test questions related to fiber optic, Gershun tube, and spectrometer performance. A Zeiss MCS series spectrograph with Hamamatsu CCD detector and Tec5 interface electronics was interfaced to a customized "Y" fiber bundle to permit light collection from either of two Gershun tube collectors optimized for either direct solar beam or scattered sky light collection. (Manufacturer and model information is provided for descriptive purposes only and does not imply recommendation or endorsement by NASA or DOE). An altitude/azimuthal pointing system was designed and fabricated, driven by identical Oriental Motor precision-grade harmonic planetary-geared stepping motors with integrated resolver feedback systems on each axis. National Instruments digitization and motion controller cards were interfaced to a rack-mount industrial PC system with Intel processor, Microsoft Windows XP operating system, and National Instruments LabView graphical data acquisition and control programming software. A second version of the instrument was built in a more flight-like configuration and included a hollow shaft motor on the azimuth axis and a coiled winding or "clockspring" mechanism for the fiber optics and electronics that connected to the light collector and shutter apparatus.

The ground prototype systems (Figure 3) performed remarkably well and most of the elements were adopted for the flight instrument design. The modular configuration permits the spectrometer, data system, and power supplies to be rack mounted and the scanning head (motors, fiber, and baffle tubes) to be quite compact. Furthermore, the custom scanning head frame components can accommodate a

variety of collection optics and fiber bundle configurations, and can be interfaced to a variety of spectrometer and detector elements that can be readily added as rack mount components.

Figure 3. Ground prototype systems. (**a**) Fiber optic test system. (**b**) "Clockspring" system.

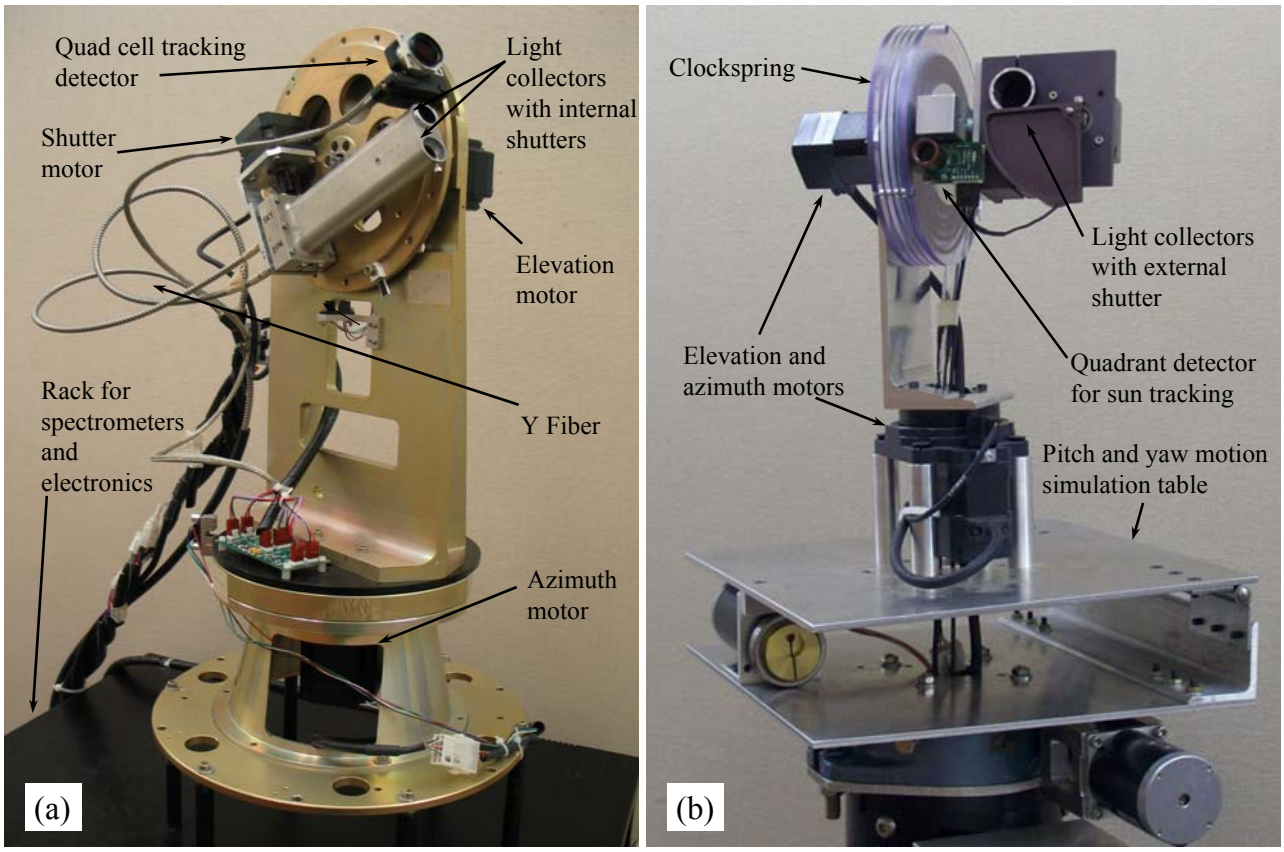

An important finding of preliminary work with this system was that the sky light collection task is a significant optical design driver. Scattered light flux from clear sky is far weaker than the direct solar beam, and the sky light collector must effectively reject the very bright direct beam radiation when the instrument is attempting to measure scattered light in the critical zone within ~5 degrees of the solar direction. Additionally, the time required to step through a reasonably comprehensive set of directional measurements along the principal plane and almucantar (perhaps 20 measurements in each dimension) is critical. Low signal levels are generally accommodated by longer integration times, but in this case both scans must be completed within ~100 s to stay within the atmospheric "cell" dimension of 10,000 m specified in Table 1 (for a nominal airspeed of 100 m/s).

The light collecting ability of a fiber optical system is limited by the fiber cross-sectional area and numerical aperture (NA), which defines the acceptance angle over which incident light will undergo total internal reflection at the core/cladding interface and be captured in the wave guide. For the direct solar beam collector, test data indicate that placing a diffuser at the fiber face helps to uniformly populate the mode structure, reduces fiber transmission anomalies, and improves the stability of individual spectral channel measurements, but significantly reduces signal levels. For the skylight collector, both mirror and lens fore-optics were tested as a means to fill the fiber numerical aperture without the use of a diffuser. This approach improved signal levels, but added direct beam crosstalk

into the sky radiance measurement within ~10 degrees of the solar direction owing to scattering from lens and mirror surfaces closer to the fiber optic end.

Additional baffle tube and shutter prototypes were built to support the compact flight instrument design. A pitch-roll-spiral-climb tilt table (Figure 3b) was designed and built to simulate the types of motion to be expected in flight and evaluate the ability of the tracking system to meet the tracking specification. Considerable work was done with these prototypes, particularly the sky light baffle tube, to achieve the best possible signal levels. A useful baseline capability has been achieved, but it is expected that further refinements to the sky light tube and fiber optic bundle may be implemented in future to continuously improve on the most challenging clear-sky and near-sun measurements.

The design of the flight instrument depicted in Figure 4 began in January 2010. The NASA design methodology and airworthiness certification process were adopted to ensure that the instrument can be used productively in the NASA Airborne Science Program and collaborating DOE flight experiments. In addition to the measurement requirements described in Table 1, design objectives included minimal intrusion into the air stream and reliable performance in a broad range of moisture, thermal, vibrational, and pressure environments. Initial certification, integration and flight testing were done in close collaboration with PNNL utilizing the DOE G-1 aircraft based at Pasco WA [12].

Figure 4. Spectrometer for Sky Scanning Sun-Tracking Atmospheric Research (4STAR) components in and above fuselage.

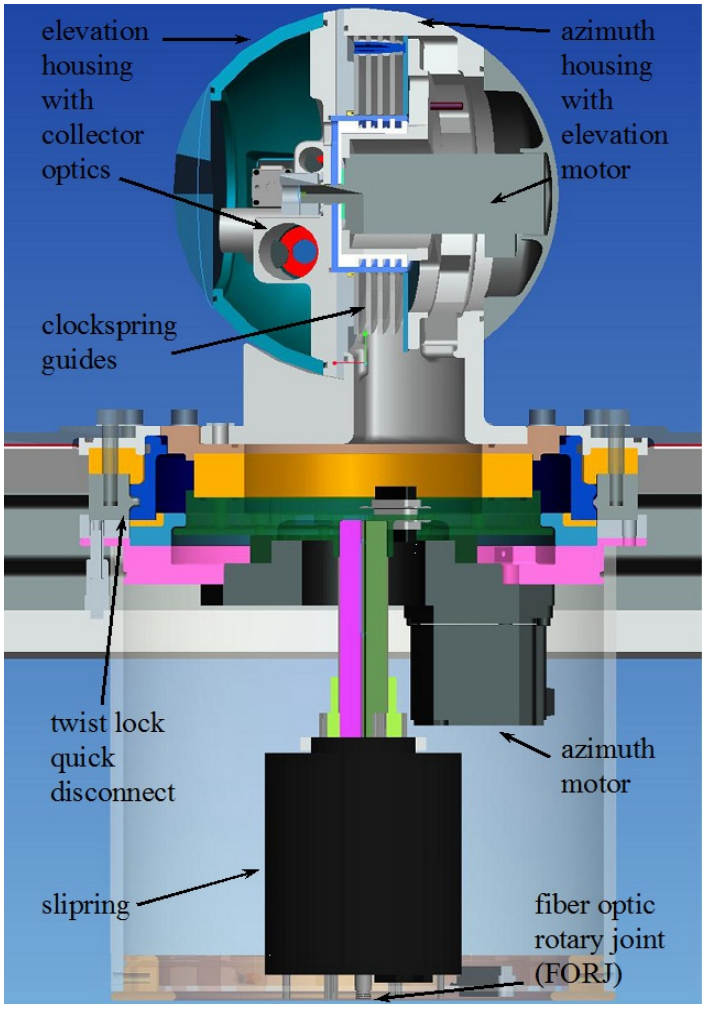

Having the baffle tube and fiber optics elements from prototype development, the flight instrument design problem was essentially one of integrating several commercially available subsystems into the smallest and most robust package (as limited by schedule and budget constraints). A split-sphere design was selected, with minimal protrusion of optical components into the air stream, to avoid high variability in air loads resulting from a non-symmetrical shape scanning through the full alt-azimuthal range of motion.

One of the more challenging optical design problems was to transmit the optical signal across two rotating interfaces. The 180° elevation axis range of motion can be achieved using a flexible coil for both the electrical and optical signals connecting to baffle tube, shutter, and quadrant detector components. The principal constraint on this coil geometry is the allowable bend radius for the fiber optic light guide, which scales linearly with the fiber core diameter. This is one important reason for using a bundle of smaller fibers rather than one large fiber. A "Y" bundle was designed, comprising 19 105-micron fibers in a hexagonal packing pattern, with three fibers dedicated to collecting the direct solar beam and 16 fibers dedicated to skylight collection. The bend radius limitation for doped-silica-clad synthetic-fused-silica fibers having the best spectral transmission properties for this application is ~40 mm. Radial coil geometry was selected with the inner end of the coil rotating with the elevation housing shaft and the outer end connected to the azimuth housing. This coil assembly is termed the "clockspring" because of its similar appearance, and fits compactly around the elevation planetary gearmotor drive in the azimuth housing. The instrument comprises four axially stacked clockspring elements; one for the fiber optic bundle and three for electrical conductors.

The spiral climb and descent maneuvers typical for vertical profiling requires continuous rotation capability on the azimuth axis. A solid core fiber optic rotary joint (FORJ) design was selected for this axis, recognizing the potential for significant azimutual variability but anticipating deterministic behavior (based on tests performed in the prototype phase) that could be corrected through azimutual calibrations. A stock 48-channel Moog hollow shaft carbon-brush slipring was specified for the electrical conductors. An Oriental Motor helical ring drive rotary actuator was specified to provide a large on-axis region to route these electrical and fiber conductors.

The instrument head must be sealed against rain and cloud water intrusion. Even water vapor in the head can be problematic if it causes fogging or frosting of optical elements, which could reduce transmission and add scattered-light noise into the measurement. Furthermore, the instrument head penetrates the pressure shell of the aircraft and must be sealed to maintain cabin pressure to ensure airworthiness. The seal design borrowed heavily from AATS heritage, using Teflon lip seals on the elevation and azimuth shafts and synthetic fused silica windows to seal the baffle tubes. Window cleanliness is a challenge, and the instrument is fitted with a quick-lock mount to permit removal for pre-flight cleaning from inside the cabin, as well as a sealed parking block (not shown) to protect the windows from heavy rain and cloud condensation during flight. The quick-lock design eliminates the need for access to the top of the aircraft prior to each flight, as was the case for the AATS instruments. All non-rotating assembly interfaces are sealed with low-temperature silicone o-rings. A dry-gas purge system was included to provide a constant low-pressure (~15 kPa) differential between the inside of the head and the static pressure outside the aircraft. This system required considerable airworthiness analysis to accommodate safe use of the compressed gas energy source as well as the more complex pressure regulation scheme required to regulate against the external static reference pressure.

3. Laboratory Testing of Flight Instrument Performance

Testing of critical components of the certified flight instrument for performance against the requirement specifications identified in Table 1 was conducted. This included evaluation of the primary spectrometer systems (detectors and grating performance), fiber optic elements, optical collectors, and tracking system.

3.1. Detector Linearity

Very high radiometric repeatability is a fundamental requirement for Sun photometry. The visible spectrometer with its CCD detector array was chosen based on the expectation of high dynamic range, without specific attention to linearity. Nonlinearity may be tolerated but must be well understood and corrected for if significant. Experimental determination of linear radiometric response can be difficult at the accuracy (repeatability) levels required for Sun photometry, and must be done in a way that is compatible with the critical Sun tracking mode of operation for the instrument. Important parameters that define this operational mode include the throughput of the light collecting system and the CCD integration time, which can be selected so that the detector element electron wells are nearly filled for maximum brightness operational modes, *i.e.*, top-of-atmosphere sun tracking. The ideal test would be to acquire data at this integration time with a precision light source having the same spectral emission shape as the sun that could be varied with high accuracy across the full dynamic range from incipient light detection through saturation. However no such ideal calibration light sources actually exist that produce accurately known radiant fluxes over the full spectral range and dynamic intensity range of the 4STAR—even for the direct solar beam. But in addition, the 4STAR is designed to measure not only direct sunlight but also diffuse skylight which may have distinctly different spectral shape than direct sunlight. Thus, determination of detector linearity of a hyperspectral instrument like the 4STAR based solely on the known calibrated radiant fluxes from existing light sources is not possible. Another approach would be to observe a very steady (not necessarily calibrated) source and vary the spectrometer integration time to fill the CCD electronic wells across the full span up to the limit of saturation. This technique does raise some questions regarding dark current and read noise effects that might not be consistent with integration time. These effects can be addressed and removed by systematically incorporating dark current measurements into the calibrations and in the instrument operational modes. There remains the question of how to apply these uncalibrated relative measurements to improve radiometric measurements which ultimately must be calibrated in some absolute sense.

Ultimately, by combining measurements of stable calibrated integrating sphere light sources operated at several distinct calibrated intensity levels with a self-referential technique in which dark current and radiant signal were measured while the spectrometer integration times were varied, we were able to accurately determine the linearity to small fractions of a percent over most of the dynamic range of our spectrometers. The left panel of Figure 5 plots the product of data rate and integration time against well depth (inferred from A/D converter range). The right panel curve normalizes this relationship against its value at 50% full well. It is instructive that data for all wavelengths and lamp power levels collapse to this right panel curve shape, so that it can be used as a look-up table to correct

each measurement as a function of only the measured digital counts. However linearity error for this CCD detector is not judged to be large enough to require correction.

Figure 5. Charge-coupled device (CCD) linearity evaluated from integrating sphere measurements by alternately varying integration time and incident light intensity. The right curve is normalized to 50% of full well.

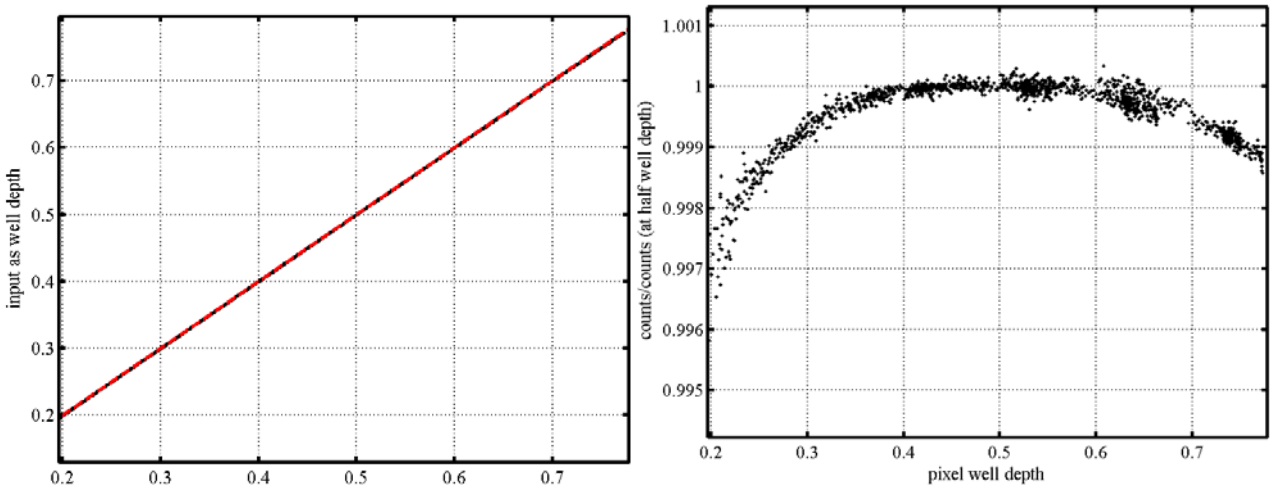

3.2. Spectral Calibration and Characterization

Spectral calibration is required to establish the relationship between detector column and the wavelength that is being measured. Manufacturers provide calibration data which can be corroborated by laboratory testing using emission line lamps, or by observing atmospheric absorption features at known wavelengths. We have chosen a direct verification test using illumination with specific known wavelengths from gas emission lamps as shown in Table 2. We evaluate spectral registration error from both the manufacturer's calibration and a more extensive calibration performed with colleagues at NASA's Goddard Space Flight Center [13]. The worst-case spectral error is 0.25 nm for the visible and near-infrared (VNIR) spectrometer and 1.21 nm for the SWIR spectrometer. Spectral line shape is another instrument parameter that is particularly important for gas absorption measurements. The fundamental physical line shape for a slit/grating type spectrometer in the far field is a sinc function having the width directly derived by slit diffraction. For the spectrometers used here, the combination of near-field and curved grating effects produces a markedly different line width and shape, which resembles a nearly symmetric Gaussian. We have measured the full width at half maximum (FWHM) using both monochromator and emission lamp sources and find that our measurements agree with the manufacturer specifications to within 15% (Figure 6). The anomaly appearing around 560 nm is judged to be physical, reflecting the effect of an order sorting filter applied to the CCD. For our trace gas analysis [14] we use the most current calibration results that determine FWHM wavelength dependency.

Table 2. Spectrometer wavelength calibration (all units are nm).

Lamp	Spectrometer			
Gas	**Wave-Length**	**Measured Column**	**From Mfg.**	**From GSFC Calibration**
VNIR Spectrometer				
Hg	365.18	239.71	365.27	365.23
Hg	404.66	288.60	404.74	404.21
Hg	435.83	327.24	435.88	435.88
Hg	546.07	464.62	546.15	546.33
Ar	696.54	654.00	696.61	696.56
Ar	763.51	739.00	763.41	763.16
Kr	811.29	800.02	811.04	811.07
Ar	912.30	931.00	912.24	912.58
Ar	965.78	1001.40	966.00	965.37
SWIR Spectrometer				
Kr	1145.75	419.16	1144.54	NA
Kr	1220.45	365.22	1219.42	NA
Kr	1317.74	295.21	1317.04	NA
Cd	1448.70	200.47	1447.68	NA
Cd	1570.80	107.71	1570.98	NA

Figure 6. Measured linewidth as a function of wavelength for the visible and near-infrared (VNIR) Spectrometer.

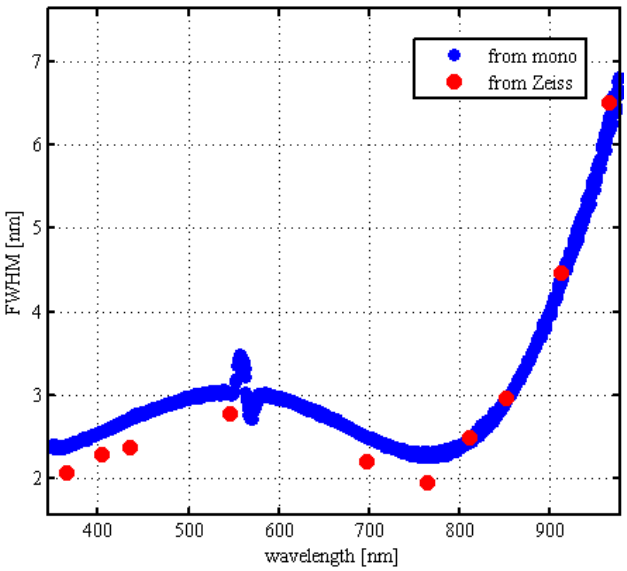

3.3. Other Detector and Spectrometer Error Sources

Other sources of error in the detectors and spectrometers that need to be addressed include dark current, thermal drift, photon statistical or "shot" noise, and stray light arising from spurious reflection or surface scattering from internal components in the optical path. Dark current appears to be relatively stable for both CCD and InGaAs photodiode array detectors and is corrected for each wavelength. Thermal drift has been managed at the detector level with customized thermoelectric cooler elements and at the op-amp signal processing level by placing the spectrometer and external processing

electronic modules in a temperature and humidity controlled chassis. This constant temperature environment has the added advantage of minimizing material expansion effects that might compromise spectral calibration. A thermal test was performed on the composite system by varying the set-point of this temperature controlled chassis while observing a constant integrating sphere light source and the results show less than 1% variance over a 5° temperature range (Figure 7). During normal operation the sealed spectrometer enclosure box temperature (measured in the internal cooling air path) is stabilized to within about 1 degree and the relative humidity is stabilized at less than 5%.

Figure 7. Detector thermal stability at several key wavelengths for the charge-coupled device (CCD) (**a**) and InGaAs (**b**) detectors.

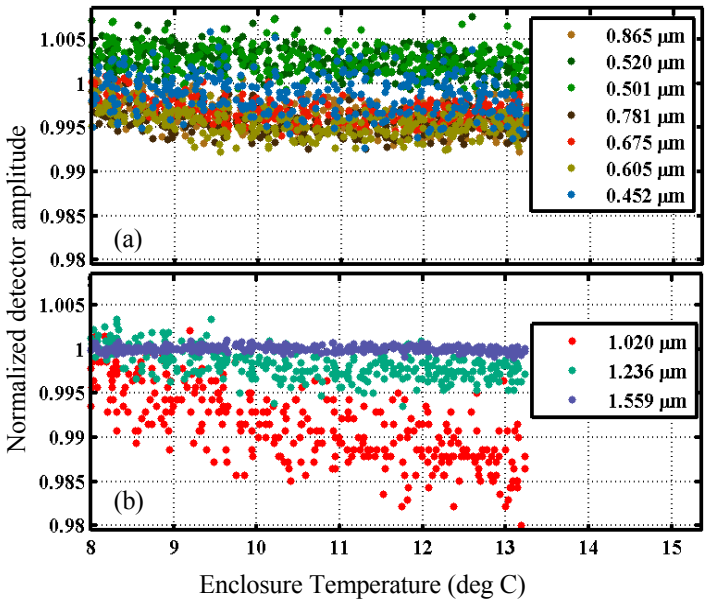

Stray light effects were found to be due to three distinct sources, both internal and external to the spectrometers: (1) distinct spectral artifacts attributed to "recycled light" internal to the spectrometer, (2) diffuse stray light attributed to finitely limited out-of-band rejection in the wings of the grating spectrometer slit function or even just to low levels of random diffuse scattering from optical surfaces within the spectrometer including the grating and even the detectors themselves, and (3) stray light external to the spectrometers due to non-zero suppression of bright sources outside of the design field-of-view. In particular, measurements of sky radiance at small scattering angles near the solar disk are susceptible to artificial enhancement due to undesired residual scattering of sunlight on optical elements.

Wavelength specific stray light (type 1) was evaluated by illuminating the spectrometer fiber-optic feed with the output from a scanning monochromator, which was scanned across the entire wavelength spectrum of light entering the system. Initial tests indicated some significant stray light problems including signal artifacts that were eventually correlated to relative humidity and led to the conclusion that this VNIR spectrometer suffered from detector frost-over or possibly de-lamination effects. The VNIR spectrometer was replaced at the same time that humidity control was added to the chassis box. The new spectrometer shows little evidence of internal stray light as shown in Figure 8 where the monochromator wavelength is plotted as a function of detector column number, with color representing the log (base 10) of the detector response normalized to peak value. Order blocking filters were selectively inserted into the monochromator output path to minimize higher order light from the

monochromator grating. The diagonal line represents essentially the spectral calibration curve. The width of this diagonal correlates to the linewidth as a function of wavelength, and any variations from dark blue in the region off this diagonal indicate stray light artifacts within the spectrometer. Both spectrometers appear to be quite free of discrete artifacts. The VNIR spectrometer shows minimal stray light down to the 0.1% level. The SWIR spectrometer does show incipient noise at the 1.0% level, but this analysis is limited by low light levels in the test data presented here.

Figure 8. Stray light artifacts for (**a**) the visible and near-infrared (VNIR) and (**b**) short wave infrared (SWIR) spectrometers.

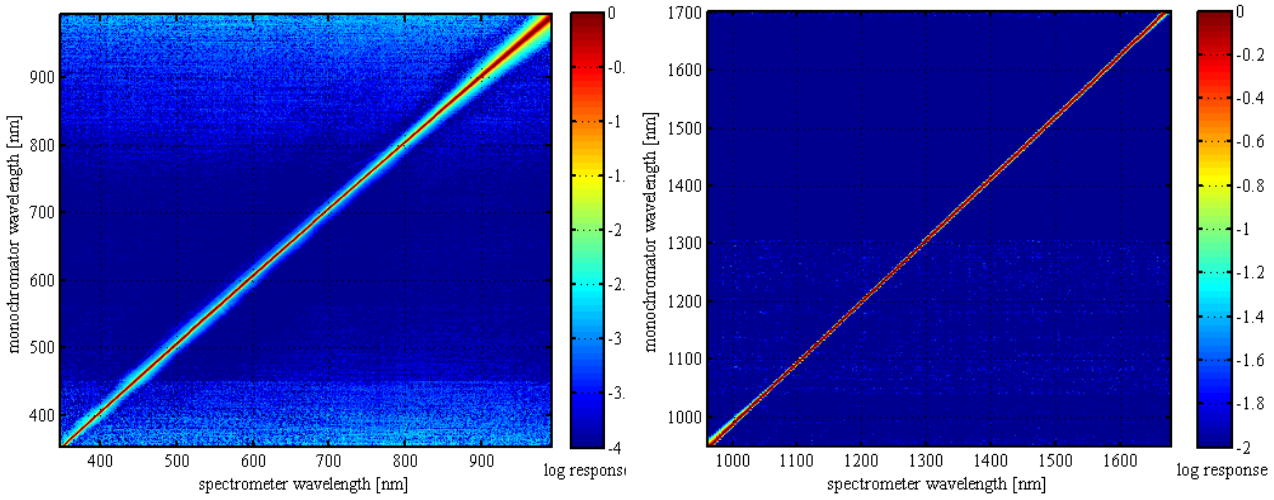

(**a**) (**b**)

A method to evaluate diffuse stray light (type 2) scattered from, e.g., the grating over the full spectral range involved the use of high pass and low pass cutoff filters (optical density > 4) to examine leakage onto the detector for the wavelength range that was known to be blocked by the filter. This leakage can be more problematic for the UV or IR regions of the spectrum where the solar illumination is weak and can be overwhelmed by even very slight scattering from the peak regions of the spectrum. This test indicates that stray light effects are less than 0.1% for wavelengths greater than 420 nm (Figure 9).

Lastly, we evaluated the effects of "type 3" stray light due to scattering from optical elements external to the spectrometers by careful in-lab measurements with bright artificial sources (collimated lasers) but also operationally by measuring sky radiance over a range of near-sun scattering angles while alternately shading or exposing the foreoptics to direct sunlight. These shaded/unshaded measurements provide a direct measure of the magnitude of artificial enhancement of sky radiance at shallow scattering angles. These are discussed in section 3.5 along with other tests of the optical system performance.

Poisson or "shot" noise is a well-understood phenomenon influencing the counting statistics of independent events (such as photon arrivals) and is known to scale as the square root of the number of counted "events". Ensemble averaging over long integration times is an acceptable way to reduce this and other types of randomly distributed noise. It is important to understand the level of these noise sources in relation to other noise sources in the system, in order to optimize the time productivity of the instrument, particularly in context of limited time available to collect a full sky scan data set as identified in Table 1. We are incorporating these concepts into more adaptive data acquisition strategies to optimize data collection to targeted levels of measurement uncertainty.

Figure 9. Scattered light artifacts in the VNIR spectrometer are quantified using long pass (LP) and short pass (SP) filters. The left curve shows the illuminating spectrum along with the filtered measurements. The right curve shows the scattered light crosstalk.

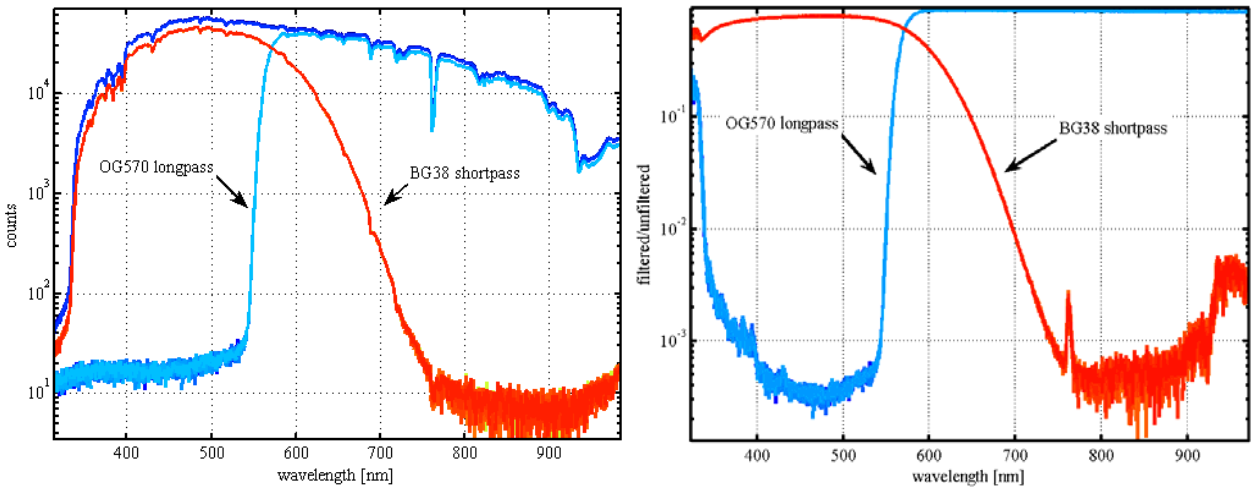

3.4. Light Path Transmission Stability

The spectral transmission of the light path must also be very stable if the instrument is to perform to specification. Sources of degradation to the throughput of the optical system include the cleanliness of the window apertures, degradation of optical materials owing to ultraviolet radiation or mechanical effects, and alignment stability. One of the more challenging optical design problems was to transmit the optical signal across two rotating interfaces corresponding to the two axes of the elevation-azimuthal tracking system. The use of fiber-optic waveguides in this design provided a compact layout with reduced system sensitivity to alignment errors but introduced optical throughput constraints as well as unanticipated physical optics effects influencing spectral transmission.

To demonstrate the radiometric stability of the fiber optic coil element, a test fixture was developed comprising a high-powered "white" light emitting diode (LED) driven at constant current and attached to a large heat sink to minimize thermally induced radiometric variability. This fixture was attached to the sunlight collector aperture and the elevation axis was scanned through its full range of motion. This test indicated that the variability resulting from flexure of the coiled fiber optic was less than 0.16% over the full range of motion (Figure 10).

The FORJ proved to be more problematic. Initial tests using integrating sphere illumination and photodiode detectors indicated that a smooth and repeatable sine wave transmission profile could be obtained. However, when the FORJ was integrated into the instrument, significant problems emerged, manifest as variability across the wavelength spectrum and hysteresis in the transmission, *i.e.*, phase lag depending on the direction of rotation. Normal sun tracking operation requires considerable dithering about the azimuthal pointing direction, therefore hysteresis represents an uncorrectable and unacceptable error mode for this component. Several different designs were built and tested, and the best result is presented in Figure 11. Normalized transmission deviation from the mean is plotted as a function of azimuth for both directions of rotation. Note the non-sinusoidal behavior with discontinuous regions as well as hysteresis, most noticeable around 100–120 and 300–320 degrees azimuth. Furthermore we determined that this discontinuous zone was not stable and repeatable over

long periods of time but might shift according to the way the instrument was handled. This component is essentially out of tolerance for the instrument specification. A field calibration workaround has been devised based on the use of the LED fixture described above to monitor the position of the hysteresis zone. Data must then be screened to eliminate data contaminated by this hysteresis problem. A longer-term solution is described in the future work discussion in Section 4. Nevertheless the data presented in Figure 11, typical of the behavior of the FORJ across all flights of a recent field campaign indicates that with data screening to avoid regions of extreme hysteresis, and lookup table corrections we can reduce this error to less than 0.5% for >75% of the azimuth range.

Figure 10. Elevation axis optical path mechanical stability is demonstrated by very low change (ordinate) for both positive and negative rotation over the full range of tracking motion with LED illumination.

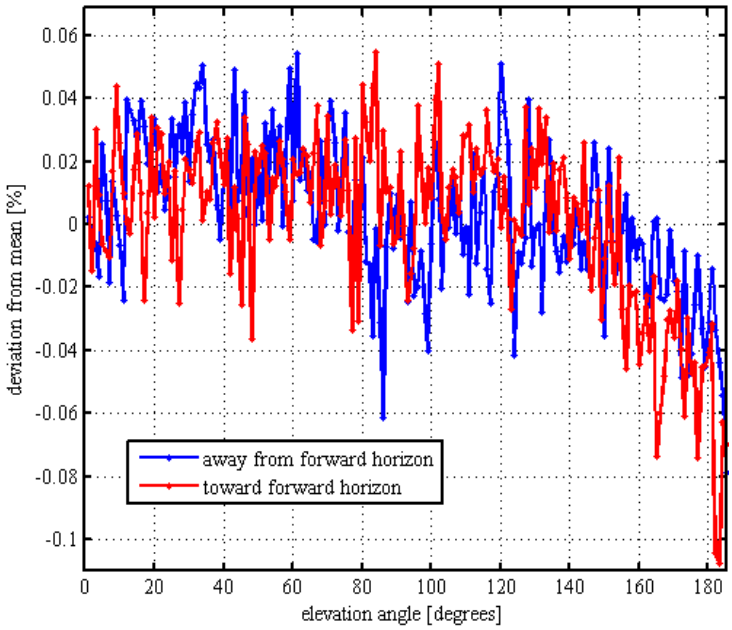

Figure 11. Fiber Optic Rotary Joint (FORJ) transmission as a function of azimuth angle.

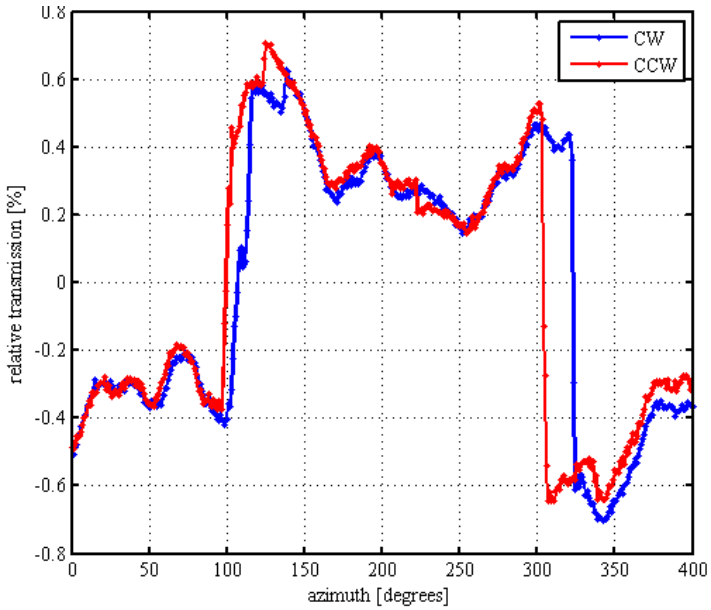

3.5. Field of View (FOV) Characterizations

Field of view (FOV) flatness is another very important optical performance parameter, particularly for the sunlight collector. The theoretical width of the field of view plateau (full width full amplitude) for this Gershun tube sunlight collector is 1.5°, providing about a degree of tolerance for the mechanical tracking system to dither about the true direction of the Sun without causing significant loss of signal strength. One can readily appreciate that the lack of flat transmission across this field of view directly translates into radiometric error. Many versions of Gershun tube designs were built and tested. Initially the face of the fiber optic bundle was used as the lower aperture of the Gershun tube, but this approach failed to fill the full numerical aperture of the fibers in the bundle and gave rise to a number of unexpected spectral effects in the data. Early on it was determined that a diffuser in front of the fiber optic was helpful to fill all the transverse modes and reduce this spectral variability but at considerable cost to signal levels. More efficient surface scattering diffusers (Figure 12a), were tested along with some power optic and fiber-optic mode scrambler designs but the best option we have tested is a thinned Spectralon volume diffuser (Figure 12b).

Figure 12. Normalized field of view flatness as a function of wavelength and scattering angle (mis-alignment with solar rays) for (**a**) surface scattering diffuser, and (**b**) thinned Spectralon volume diffuser. Color deviation from the orange level corresponding to 1.0 will introduce false radiometric variability as aircraft motion varies the scattering angle.

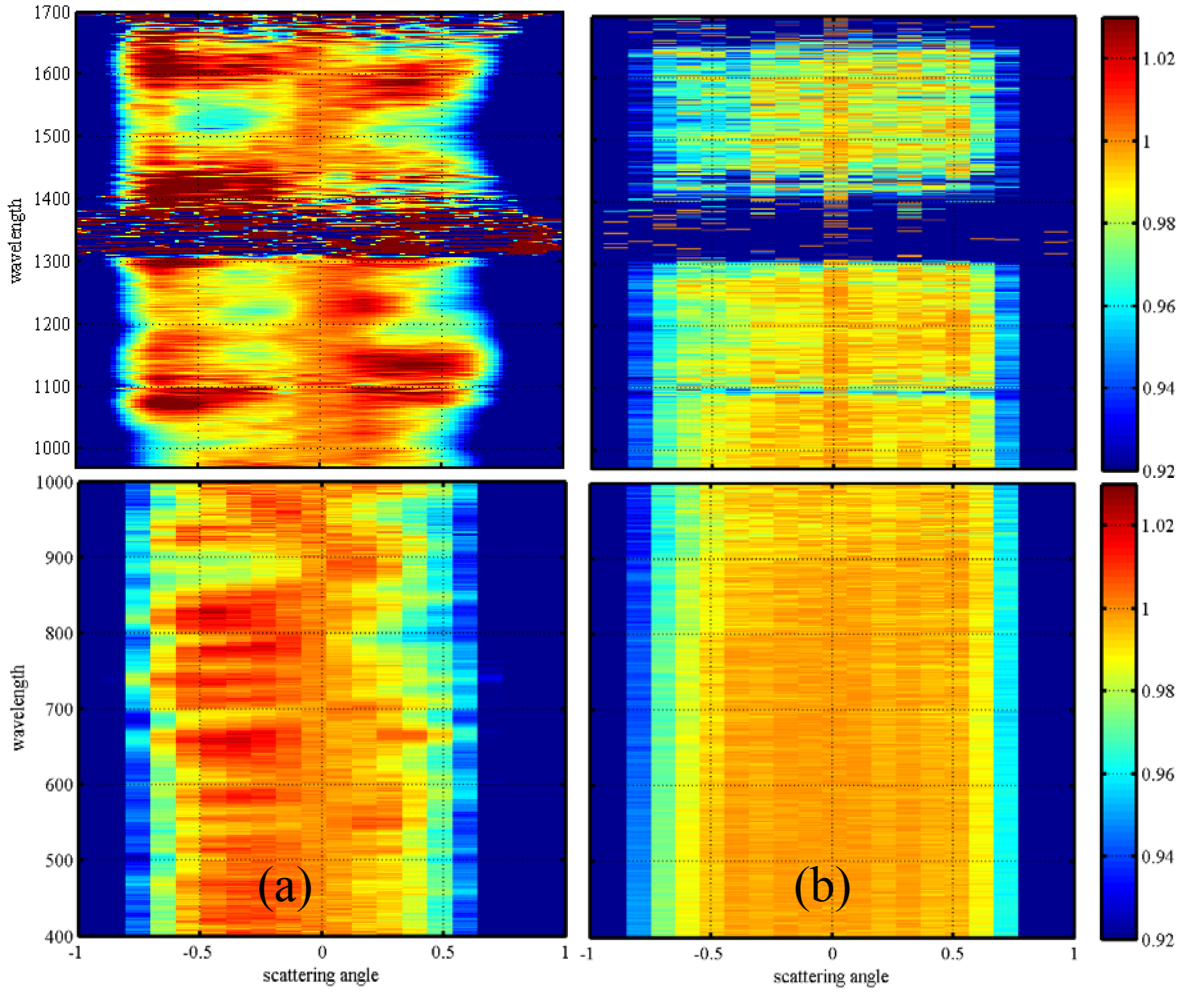

The skylight collector of the ground prototype was configured first as a Gershun tube and then as a Cassegrain telescope to provide better light collection free of chromatic aberration. The final flight instrument design utilized a simple plano-convex synthetic fused silica lens, providing the maximum light collection aperture and accepting both spherical and chromatic aberration to be within required levels for the field-of-view specification. This design provided more than 50 times the light collection capability of the Gershun tube but resulted in a very non-uniform field of view. However, this non-uniformity will not produce un-acceptable error owing to the relatively flat angular distribution of skylight intensity.

Another very significant noise source for the skylight collection measurement arises from the direct solar irradiance scattered by contamination on the skylight collector window into the skylight collection optical path (type 3 stray light as discussed in Section 3.3). Considerable effort was invested to derive a design that would minimize contamination of this critical window. The final design approach comprises a parking block that mates to a silicone seal to protect the window during flight conditions where precipitation or other airborne contaminants are known to be present. Contamination of the skylight collector window during flight operations and data collection continues to be a challenge. A test technique based on shadowing the skylight collection aperture was devised to evaluate the level of window-scattered contamination. Figure 13 shows the results of this test for very clean window conditions. Noticeable light contamination can be observed particularly in the angular region very close to the sun. A sensitivity study was conducted to evaluate the effect of this level of error on the final aerosol properties extraction and the results were found to be within acceptable limits [15].

Figure 13. Sky light contamination from direct beam scattering. Left plot shows angular effect at several wavelengths. Right plot shows wavelength dependency for several angles.

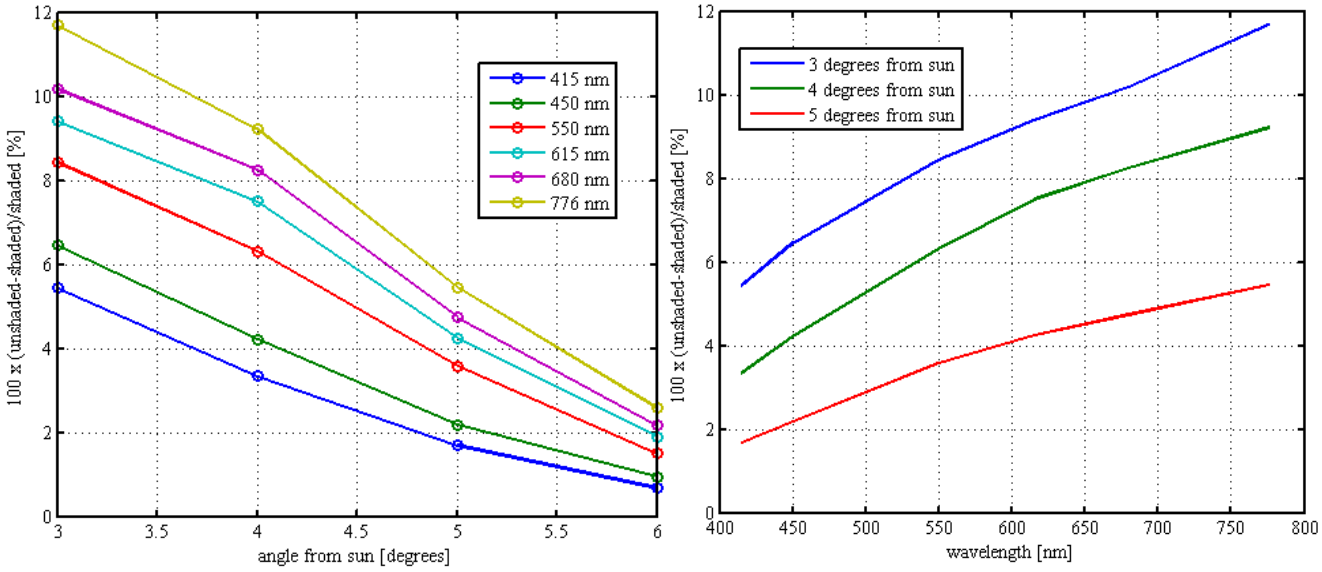

3.6. Tracking Errors

The tracking performance of the mechanical pointing system is affected by factors that include pressure seal drag, inertia, and motion control software latencies, and is intrinsically unstable for tracking conditions where the sun is located on the axis of either motor, (practically this is only an

issue for angles within about 10 degrees of the azimuth axis). Tracking performance was evaluated by measuring the phase lag of the system in a constant rotation mode. Test results indicate a phase lag of approximately 100 ms resulting in a misalignment of about 0.6 degrees for a 6° per second spiral climb maneuver, at moderate elevation angles. This is within the acceptable range of the sunlight collector field of view. Analysis indicates this phase lag is dominated by software latencies that are specific to the position-based motion control strategy employed and may be improved with velocity-based algorithms.

3.7. Radiometric Calibration

The calibration strategy for this instrument relies on AATS heritage for direct solar measurements and looks to the techniques developed by the AERONET group for calibrating skylight spectral radiance. The NASA Ames Sunphotometry group has long relied on the high-mountain Langley method [16] using the scatter of Langley plot intercept values as a measure of experimental error, calibrating before and after each flight experiment to further document the long term stability of the measurement system. Spectral radiance calibrations for the skylight collector must rely on an integrating sphere or similar light source. A third calibration process is required for gas detection measurements, which requires a continuum light source to provide calibrated spectral irradiance to supplement the solar spectrum across the atmospheric absorption features, in order to properly scale the absorption depth at these critical wavelengths. A NIST traceable quartz halogen FEL lamp source provided continuum illumination across the absorption feature, which was then interpolated across the absorption deficit in the measured solar spectrum.

Figure 14. (**a**) Example Langley plot fit for 500.8 nm, taken during the ground-based calibration campaign in Mauna-Loa, 18 December 2012. Data filtered based on twice the standard deviation from fitted line, intercept value represents the exo-atmospheric calibration value (C_0) at the 500.8 nm wavelength, and (**b**) the corresponding wavelength dependence of C_0.

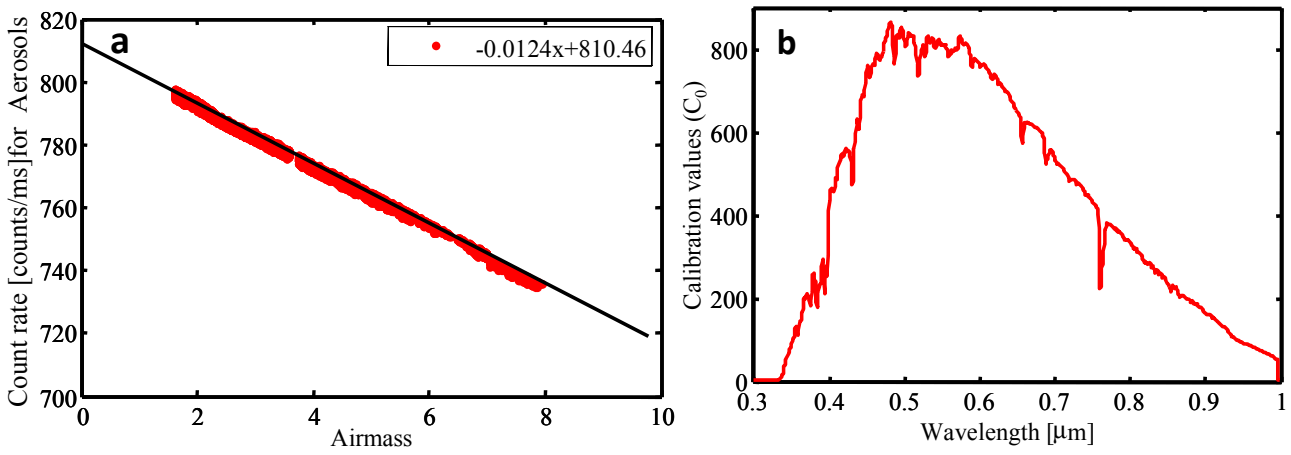

High-mountain Langley calibrations are very expensive and must be accumulated over a history of field campaigns to build confidence in the long-term radiometric stability of the instrument. Continuous improvement of several 4STAR subsystem components directly impacting the radiometric efficiency of the instrument have confounded attempts to build a long term record of consistent

Langley calibrations. Plots from the last Langley calibration are presented in Figure 14, and illustrate the degree of linearity (indicating a nearly pure Raleigh atmosphere) as well as the wavelength dependency of the calibration intercept (top of atmosphere voltage) C_0. Skylight spectral radiance is calibrated to provide a conversion between the detector readout and at-sensor radiance. The radiance standard for this calibration is the NASA Ames Airborne Sensor Laboratory 36" sphere, calibrated to NIST traceability [17] Figure 15 illustrates the spectral response curves for the two spectrometers.

Figure 15. Sky radiance calibrations for the (**a**) visible and near-infrared (VNIR) and (**b**) short wave infrared (SWIR) spectrometers.

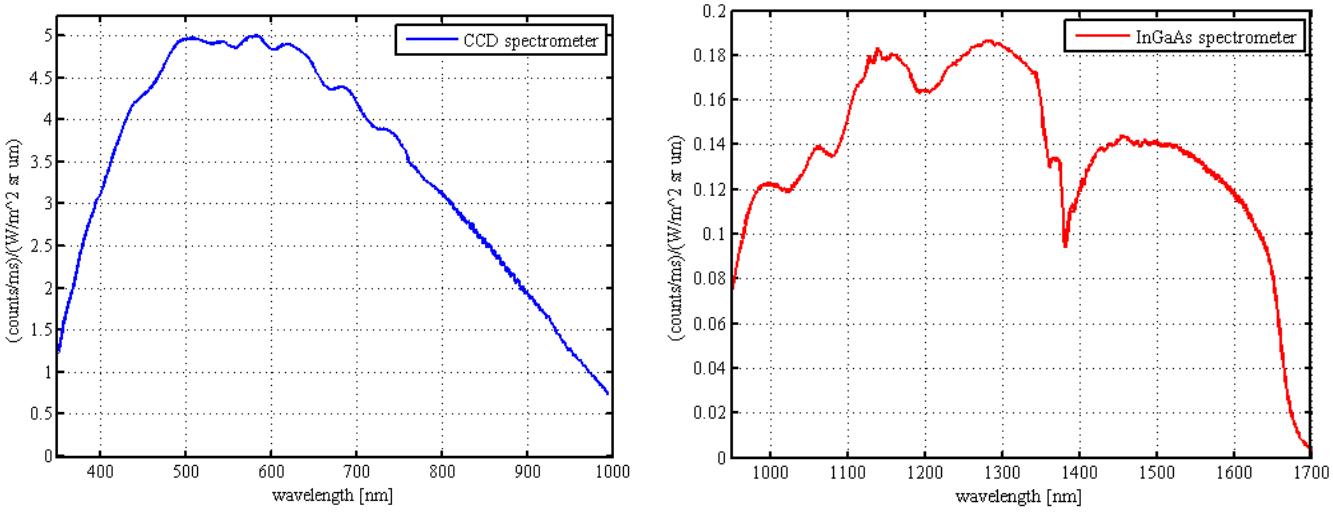

(**a**) (**b**)

3.8. Flight Testing

The flight instrument has been tested in a series of engineering flights conducted in September 2010, April 2011, and August 2011. The certified instrument (shown during Mauna Loa Observatory (MLO) calibration in Figure 16a) was installed on the DOE Gulfstream G-1 aircraft (Figure 16b) and flown for more than 15 h at altitudes up to 5,950 m. Test objectives centered on airworthiness certification and the functional demonstration of tracking and direct beam measurement capability. The instrument met all test objectives for sun tracking measurement and provided considerable data to evaluate performance.

Following this certification flight series the instrument was deployed in both phases of the DOE Two Column Aerosol Project (TCAP) mission in summer 2012 and winter 2013, logging more than 100 flight hours of operation. Both aerosol optical depth and gas absorption measurements were made during this flight experiment. Example data are shown in Figures 17 and 18 and described in scientific context in complementary publications [14,18] respectively.

Figure 16. Spectrometer for Sky Scanning Sun-Tracking Atmospheric Research (4STAR) instrument (**a)** photographed during Langley calibration at Mauna Loa Observatory and (**b**) mounted in the Department of Energy G-1 aircraft (appearing as black sphere atop fuselage).

Figure 17. Aerosol optical depth and extinction coefficient vertical profiles from Two Column Aerosol Project (TCAP)-1 flight experiment.

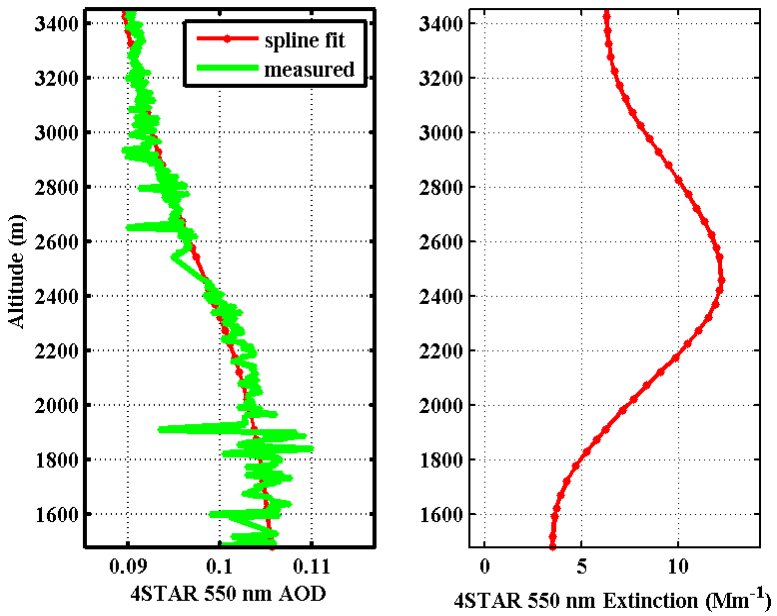

Figure 18. Water vapor density (WVD) retrieved values from Spectrometer for Sky Scanning Sun-Tracking Atmospheric Research (4STAR) (magenta) and the *in situ* G-1 hygrometer (blue) for a spiral ascent during the 25 July 2012 Two Column Aerosol Project (TCAP) flight, with WVD difference (solid black) on upper axis.

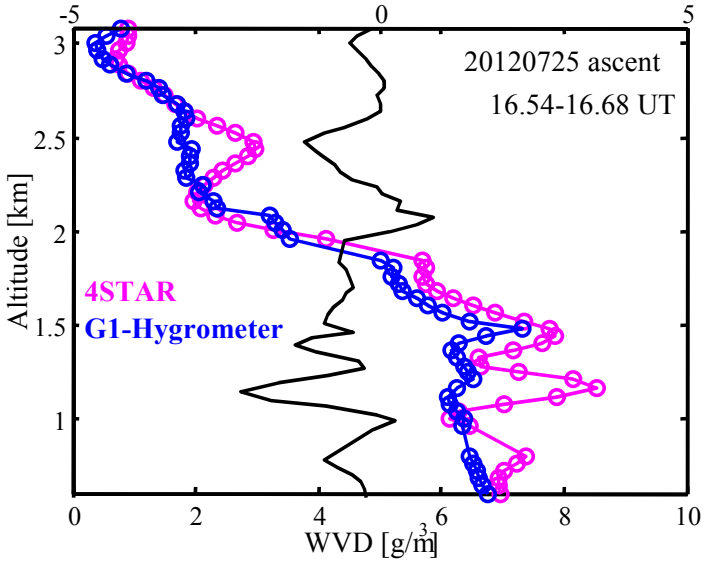

4. Future Work

Basic limitations in the performance of the fiber optic rotary joint will require that this component be replaced in the near future. The current plan is to implement another coiled fiber device on the azimuth axis providing ± three revolutions of control authority. This will introduce the operational requirement to suspend data collection and unwind the coil during normal spiral flight maneuvers, at some slight cost to data collection duty cycle. However the improved radiometric stability of this design overshadows the drawbacks of minor data loss and operational complexity.

Further, it is recognized that a field calibration standard will be quite valuable to complement the Langley calibration method, particularly as the fiber optic light path must be disconnected and reconnected several times during the course of deployments. Both light source and detector standards are useful in this context. Photodiode array detectors operated alongside the 4STAR looking at the same (solar or integrating sphere) source represent a very attractive detector standard which is expected to be very reliable and repeatable, provided proper thermal stabilization is achieved. Recent developments of light emitting diode (LED) sources, spectrally mixed to more closely resemble the solar spectrum and interfaced to appropriate integrating sphere or diffuser stack optical elements [19] may provide a useful field calibration capability. Other light source standard options include RF and laser excited plasma light sources, which are emerging as highly stable and repeatable radiometric standards.

5. Conclusions

A new airborne sunphotometer has been designed, fabricated, and tested by the National Aeronautics and Space Administration (NASA) Ames Sunphotometer-Satellite Team working in collaboration with the Pacific Northwest National Laboratory (PNNL)'s Atmospheric Sciences and

Global Change Division, and NASA Goddard's AErosol RObotic NETwork (AERONET) team. The instrument builds on the heritage of previous NASA instruments but incorporates radically different technology for most of the major subsystems. Improved measurement capabilities include many more spectral channels, with fine enough spectral resolution to study gas constituent absorption as well as aerosols. Furthermore, a separate optical collector has been added to permit sky scattered light collection over the full principal plane and almucantar angular domain. This instrument permits the extension of the ground-based AERONET measurement capability [20] to include vertical profiling and horizontal-transect mapping from aircraft, *i.e.*, a mobile AERONET capability.

The new instrument has been engineered, fabricated, and certified for flight. Certification included a number of tests to directly address the challenges identified in Section 2. The charge-coupled device (CCD) detectors have adequate sensitivity. Long term stability remains to be demonstrated using a fixed instrument configuration over an ensemble of high-mountain Langley calibrations. With proper optimization of the sky scanning profile, the light collection capability of the optical system provides adequate photon flux to complete sky scans within a reasonable time and spatial region. Stray light within the spectrometers is within acceptable limits. Fiber optic flexible coil elements provide stable radiometric transmission over the required angular domain, but the fiber optic rotary joint transmission is degraded by regions of hysteresis that introduce non-repeatable variability on the order of 1%–2%. Window cleanliness is adequate for the direct solar measurement mode but may be problematic for skylight measurements owing to direct beam scattering, particularly for small solar angles. However, this error is not expected to prohibit useful aerosol type and size characterization. Finally, the pressurized cabin seals and tracking drive mechanisms are capable of adequate tracking response, even without implementing potential improvements to the control algorithms.

A series of engineering flights were conducted to bring the instrument to mission readiness, to support NASA and the Department of Energy (DOE) Airborne Science missions as well as the calibration and validation of earth observing systems that measure the effects of aerosol and molecular absorption on the Earth's radiation budget. The instrument has successfully supported the DOE Two Column Aerosol Project (TCAP) missions in summer 2012 and winter 2013, providing both aerosol optical depth and gas absorption measurements critical to the mission objectives. A few important instrument enhancements and field calibration methodologies are anticipated to address the objective of continuously improving the radiometric stability and accuracy of this measurement capability.

Acknowledgments

4STAR design, development, and testing were supported by the NASA Radiation Science Program, the Ames Instrument Working Group, the DOE Atmospheric Radiation Measurement Program, Battelle's Pacific Northwest Division, and the NOAA Office of Global Programs. Instrument conceptual advice and scientific data analysis software were provided by the NASA Goddard AERONET group under the leadership of Brent Holben.

Conflict of Interest

The authors declare no conflict of interest.

References

1. Schmid, B.; Redemann, J.; Russell, P.B.; Hobbs, P.V.; Hlavka, D.L.; McGill, M.J.; Holben, B.N.; Welton, E.J.; Campbell, J.R.; Torres, O.; *et al.* Coordinated airborne, spaceborne, and ground-based measurements of massive, thick aerosol layers during the dry season in southern Africa. *J. Geophys. Res.* **2003**, doi: 10.1029/2002JD002297.
2. Livingston, J.; Schmid, B.; Redemann, J.; Russell, P.B.; Ramirez, S.A.; Eilers, J.; Gore, W.; Howard, S.; Pommier, J.; Fetzer, E.J.; *et al.* Comparison of water vapor measurements by airborne Sun photometer and near-coincident *in situ* and satellite sensors during INTEX/ITCT 2004. *J. Geophys. Res*. **2007**, doi: 10.1029/2006JD007733.
3. Livingston, J.M.; Schmid, B.; Russell, P.B.; Eilers, J.; Kolyer, R.W.; Redemann, J.; Ramirez, S.A.; Yee, J.-H.; Swartz, W.H.; Trepte, C.R.; *et al.* Retrieval of ozone column content from airborne Sun photometer measurements during SOLVE II: Comparison with coincident satellite and aircraft measurements. *Atmos. Chem. Phys*. **2005**, *5*, 2035–2054.
4. Russell, P.B.; Livingston, J.M.; Redemann, J.; Schmid, B.; Ramirez, S.A.; Eilers, J.; Khan, R.; Chu, A.; Remer, L.; Quinn, P.K.; *et al.* Multi-grid-cell validation of satellite aerosol property retrievals in INTEX/ITCT/ICARTT 2004. *J. Geophys. Res*. **2006**, doi: 10.1029/2006JD007606.
5. Schmid, B.; Ferrare, R.; Flynn, C.; Elleman, R.; Covert, D.; Strawa, A.; Welton, E.; Turner, D.; Jonsson, H.; Redemann, J.; *et al.* How well do state-of-the-art techniques measuring the vertical profile of tropospheric aerosol extinction compare? *J. Geophys. Res*. **2006**, doi: 10.1029/2005JD005837.
6. Shinozuka, Y.; Redemann, J. Horizontal variability of aerosol optical depth observed during the ARCTAS airborne experiment. *Atmos. Chem. Phys.* **2011**, *11*, 8489–8495.
7. Shinozuka, Y.; Redemann, J.; Livingston, J.M.; Russell, P.B.; Clarke, A.D.; Howell, S.G.; Freitag, S.; O'Neill, N.T.; Reid, E.A.; Johnson, R.; *et al.* Airborne observation of aerosol optical depth during ARCTAS: Vertical profiles, inter-comparison and fine-mode fraction. *Atmos. Chem. Phys.* **2011**, *11*, 3673–3688.
8. Colarco, P.R.; Toon, O.B.; Reid, J.S.; Livingston, J.M.; Russell, P.B.; Redemann, J.; Schmid, B.; Maring, H.B.; Savoie, D.; Welton, E.J.; *et al.* Saharan dust transport to the Caribbean during PRIDE: 2. Transport, vertical profiles, and deposition in simulations of *in situ* and remote sensing observations. *J. Geophys. Res.* **2003**, doi: 10.1029/2002JD002659.
9. Redemann, J.; Zhang, Q.; Schmid, B.; Russell, P.B.; Livingston, J.M.; Jonsson, H.; Remer, L.A. Assessment of MODIS-derived visible and near-IR aerosol optical properties and their spatial variability in the presence of mineral dust. *Geophys. Res. Lett.* **2006**, doi: 10.1029/2006GL026626.
10. Publications from Ames Airborne Tracking Sunphotometers. Available online: http://geo.arc.nasa.gov/sgg/AATS-website/AATS6&14Pubs.pdf (accessed on 28 July 2013).
11. Parr, A.; Datla, R.; Gardner, J. *Optical Radiometry*; Elsevier Science: Philidelphia, PA, USA, 2005; p. 188.
12. Schmid, B.; Tomlinson, J.M.; Hubbe, J.M.; Comstock, J.M.; Mei, F.; Chand, D.; Pekour, M.S.; Kluzek, C.D.; Andrews, E.; Biraud, S.C.; *et al.* The DOE ARM aerial facility. *Bull. Amer. Meteor. Soc*. **2013**, submitted.

13. Herman, J.; Cede, A.; Spinei, E.; Mount, G.; Tzortziou, M.; Abuhassan, N. NO_2 column amounts from ground-based Pandora and MFDOAS spectrometers using the direct-sun DOAS technique: Intercomparisons and application to OMI validation. *J. Geophys. Res.* **2009**, *114*, 1–20.
14. Segal-Rosenheimer, M.; Russell, P.B.; Schmid, B.; Redemann, J.; Livingston, J.M.; Flynn, C.J.; Johnson, R.R.; Dunagan, S.E.; Shinozuka, Y.; Herman, J.; *et al.* Tracking elevated pollution layers with a newly developed hyperspectral sun/sky sepctrometer (4STAR): Results from TCAP 2012 and 2013 Campaigns. *J. Geophys. Res.* **2013**, in preparation.
15. Kassianov, E.; Flynn, C.; Redemann, J.; Schmid, B.; Russell, P.B.; Sinyuk, A. Initial assessment of the spectrometer for sky-scanning, sun-tracking atmospheric research (4STAR)-based aerosol retrieval: Sensitivity study. *Atmosphere* **2012**, *3*, 495–521.
16. Schmid, B.; Michalsky, J.; Halthore, R.; Beauharnois, M.; Harrison, L.; Livingston, J.; Russell, P.B.; Holben, B.; Eck, T. Evaluation of the applicability of solar and lamp radiometric calibrations of a precision Sun photometer operating between 300 and 1,025 nm. *Appl. Opt*. **1998**, *37*, 3923–3941.
17. Source: Hiss ARC High Output Sphere. Available online: http://spectral.gsfc.nasa.gov/docs/Cal/Other/Hiss/2013/ (accessed on 28 July 2013.)
18. Shinozuka, Y.; Johnson, R.R.; Flynn, C.J.; Russell, P.B.; Schmid, B.; Redemann, J.; Dunagan, S.E.; Kluzek, C.D.; Hubbe, J.M.; Segal-Rosenheimer, M.; *et al.* Hyperspectral aerosol optical depths from TCAP flights. *J. Geophys. Res.* **2013**, in preparation.
19. Fryc, I.; Brown, S.W.; Eppeldauer, G.P.; Ohno, Y. LED-based spectrally tunable source for radiometric, photometric, and colorimetric applications. *Opt. Eng.* **2005**, *44*, 111309.
20. Holben, B.N.; Tanré, D.; Smirnov, A.; Eck, T.F.; Slutsker, I.; Abuhassan, N.; Newcomb, W.W.; Schafer, J.S.; Chatenet, B.; Lavenu, F.; *et al.* An emerging ground-based aerosol climatology: Aerosol optical depth from AERONET. *J. Geophys. Res*. **2001**, *106*, 12067–12097.